Tectonophysics 627 (2014) 122–134

Contents lists available at ScienceDirect

Tectonophysics

journal homepage: www.elsevier.com/locate/tecto

Seismically constrained thermo-rheological structure of the eastern Tibetan margin: Implication for lithospheric delamination

Lin Chen [a,*], Fredrik Berntsson [b], Zhongjie Zhang [a], Peng Wang [c,d], Jing Wu [a], Tao Xu [a]

[a] State Key Laboratory of Lithospheric Evolution, Institute of Geology and Geophysics, Chinese Academy of Sciences, Beijing 100029, China
[b] Linköping University, Linköping S 581 83, Sweden
[c] Guangzhou Institute of Geochemistry, Chinese Academy of Sciences, Guangzhou 510640, China
[d] University of Chinese Academy of Sciences, Beijing 100049, China

ARTICLE INFO

Article history:
Received 27 April 2013
Received in revised form 5 October 2013
Accepted 3 November 2013
Available online 12 November 2013

Keywords:
Lithosphere rheology
Temperature
Seismic velocity
Eastern Tibetan margin
Delamination

ABSTRACT

The eastern Tibetan margin bordered by the Longmen Shan range exhibits significant lateral differences in the lithospheric structure and thermal state. To investigate the roles of these differences in mountain building, we construct a thermo-rheological model along a wide-angle seismic profile across the eastern Tibetan margin based on recent seismic and thermal observations. The thermal modeling is constrained by the surface heat flow data and crustal P wave velocity model. The construction of the rheological envelopes is based on rock mechanics results, and involves two types of rheology: a weak case where the lower crust is felsic granulite and the lithospheric mantle is wet peridotite, and a strong case where the lower crust is mafic granulite and the lithospheric mantle is dry peridotite. The results demonstrate: (1) one high-temperature anomaly exists within the uppermost mantle beneath eastern Tibet, indicating that the crust in eastern Tibet is remarkably warmer than that in the Sichuan basin, and (2) the rheological strength of the lithospheric mantle beneath eastern Tibet is considerably weaker than that beneath the Sichuan basin. The rheological profiles are in accord with seismicity distribution. By combining these results with the observed crustal/lithospheric architecture, Pn velocity distribution and magmatism in the eastern Tibetan margin, we suggest that the delamination of a thickened lithospheric mantle root beneath eastern Tibet is responsible for the growth of the eastern Tibetan margin.

1. Introduction

The lateral rheological contrast in the continental lithosphere is a key factor controlling the behavior of continental deformation (Ranalli and Adams, 2013). Thus, knowledge of lithospheric rheological structure is fundamental to understanding the geodynamic process at the conjunct zone of different tectonic units, especially the interaction zone between mountain and basin. Both observation and modeling show that the rheology of the continental lithosphere varies with depth, characterized by alternating brittle and ductile layers with one or more brittle–ductile transitions (Ranalli and Murphy, 1987). There are two primary competing rheological models for the long-term strength of continental lithosphere, which have been termed "jelly sandwich" and "crème brulée" (Burov, 2010; Burov and Watts, 2006; Jackson, 2002). The former argues that a relatively strong and brittle upper crust is separated from a strong uppermost mantle by a weak ductile lower crust (Chen and Molnar, 1983). The latter suggests that the strength of continental lithosphere resides only in the upper part of the lithosphere, which overlies a ductile lithospheric mantle (Jackson, 2002; Jackson et al., 2008; Maggi et al., 2000a, 2000b). The lower crust may or may not have rheological strength, which depends on the geological age of the study area (Maggi et al., 2000a, 2000b). Recent studies show that these two models most likely represent two end members of a continuous spectrum of rheological behaviors, depending on the composition and temperature (Afonso and Ranalli, 2004; Pauselli et al., 2010). In fact, the rheology of the continental lithosphere not only varies with depth, but also significant lateral variations in the rheological properties can arise from different lithospheric structures, compositions and thermal regimes. Such lateral rheological variation of the continental lithosphere may play an important role in the behavior of the lithosphere deformation (Cloetingh and Burov, 1996; Pauselli et al., 2010; Tejero and Ruiz, 2002; Wang, 2001).

The eastern Tibetan margin adjacent to the Sichuan basin (see Fig. 1) is an ideal place for studying the lateral variation in the lithospheric rheology due to the lateral differences of the lithospheric structure and thermal state (Hu et al., 2011; Z. Li et al., 2012; Robert et al., 2010; Wang et al., 2007; Xu et al., 2011a; Zhang et al., 2009; Z. Zhang et al., 2010). During past decades, various observations, such as surface heat flow, gravity, seismicity and crustal velocity structure, have been accumulated in this region (Hu et al., 2000; Jiang and Jin, 2005; Wang et al., 2007; Xu et al., 2011b; J.S. Zhang et al., 2010). These data make such a study become possible. In this paper, we first briefly review the geological setting and geophysical observations on the

* Corresponding author. Tel.: +86 10 82998345; fax: +86 10 82998229.
E-mail address: sinica.lin@gmail.com (L. Chen).

0040-1951/$ – see front matter © 2013 Elsevier B.V. All rights reserved.
http://dx.doi.org/10.1016/j.tecto.2013.11.005

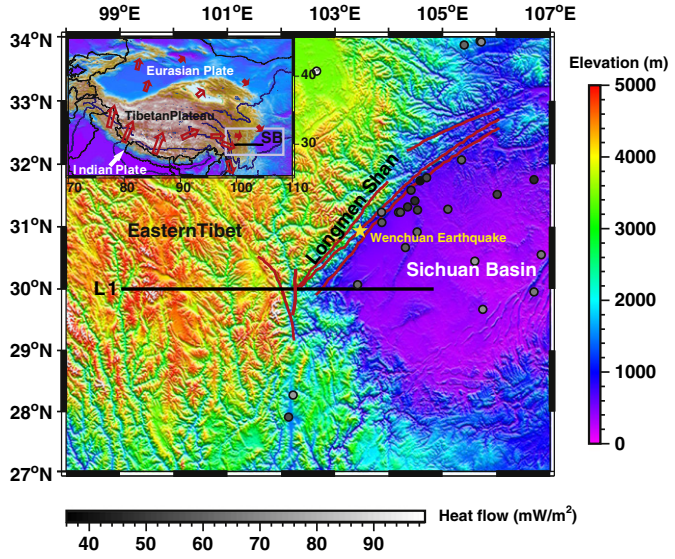

Fig. 1. Topographic map of the eastern Tibetan margin adjacent to the Sichuan basin. The solid black line, labeled as L1, shows the location of the wide-angle seismic profile reported by Wang et al. (2007). The gray-scaled points show the available heat flow observations in this region (Hu et al., 2000; Xu et al., 2011a). The red lines denote the main faults in the area. The yellow star indicates the epicenter of the 2008 Wenchuan earthquake. The inset image in the top left corner is a map of the Tibetan Plateau and its surrounding area. The white arrow shows the movement direction of Indian plate relative to Eurasian plate, which causes the southeastern extrusion of the Tibetan lithosphere. The red arrows indicate GPS vectors (Gan et al., 2007).

crustal/lithospheric structure and thermal state in the eastern Tibetan margin. Next, we describe the data set used in the study, which provide the compositional, structural and thermal information of the study region and form the basis of the construction of the 2D lithospheric thermo-rheological model. The approaches and parameters used for 2D thermo-rheological modeling are presented in the next section. Finally, the results and their possible implication are discussed.

2. Geological setting

The eastern margin of the Tibetan Plateau adjacent to the Sichuan basin is a transitional zone between the Tibetan Plateau and Yangtze craton. This margin is bordered by the NE–SW trending Longmen Shan (LMS) range with the Songpan–Ganze terrane to the west and the Sichuan basin (part of the Yangtze craton) to the east (Fig. 1). It is characterized by a sharp topography gradient from ~500 m in the Sichuan basin to more than 5000 m in the plateau over a horizontal distance less than 50 km. The eastern Tibetan margin has experienced a prolonged and complex tectonic evolution history (Burchfiel et al., 1995; Chen et al., 1995; Li et al., 2003). Its deformation was initiated in the Middle to Late Triassic in response to the amalgamation of the North China, South China and Qiangtang continental blocks (Burchfiel et al., 1995; Chen and Wilson, 1996; Li et al., 2003; Z.-W. Li et al., 2012; Liu et al., 2009). The Cenozoic deformation of the Longmen Shan was superimposed on the preexisting Mesozoic orogen (Burchfiel et al., 2008), which was reactivated by the far-field effect of the Indian–Asian collision (Harrison et al., 1992; Royden et al., 2008). The opinions concerning the timing of the Indian–Asian collision vary (Aitchison et al., 2007; Molnar and Stock, 2009; Xia et al., 2011; Zhu et al., 2013), but most researchers agree that it occurred between 55 and 45 Ma, conspicuously evidenced by a slow-down of convergence rate from over 100 mm/yr to about 50 mm/yr around 50 Myr ago (Zahirovic et al., 2012). As Indian–Asian convergence continued, the eastward growth of the Tibetan Plateau was strongly resisted by the cratonic Sichuan basin, contributing a further uplift of the eastern Tibetan margin. Although the formation mechanism of the eastern Tibetan margin is still controversial (Chen et al., 2013a, 2013b; Clark and Royden, 2000; Hubbard and Shaw, 2009; Royden et al., 2008), it is generally believed that the present high topography of the Longmen Shan and the eastern Tibetan Plateau was probably not developed until the Late Cenozoic (Arne et al., 1997; Burchfiel et al., 2008; Godard et al., 2009; Kirby et al., 2002; Z.-W. Li et al., 2012; Wang et al., 2012). However, both geological survey and GPS measurements indicate that active shortening rate across the Longmen Shan is less than 3 mm/yr (Burchfiel et al., 2008; Densmore et al., 2007; Gan et al., 2007). In addition, the Longmen Shan lacks a significant Late Cenozoic foreland basin in the Sichuan basin (Burchfiel et al., 1995). These observations suggest that the crustal shortening in the eastern Tibetan margin mainly occurred at depth and the crust here is Airy-compensated (Burchfiel et al., 2008).

Recent seismic studies reveal that great differences in crustal and lithospheric structure and property exist between the eastern Tibet and the Sichuan basin (Y. Chen et al., 2013; Hu et al., 2012; Robert et al., 2010; Wang et al., 2007; Zhang et al., 2009; Z. Zhang et al., 2010). The crustal thickness decreases from ~60 km beneath eastern Tibet to ~40 km beneath the Sichuan basin. There is an abrupt Moho offset as large as 15–20 km over a horizontal distance of ~70 km beneath the LMS (Robert et al., 2010; Zhang et al., 2009). The Moho offset may have a deep origin. Receiver function results demonstrate that the lithosphere–asthenosphere boundary (LAB) beneath eastern Tibet is remarkably shallower than that beneath the Sichuan basin with a sudden change also occurring at the LMS, although the results reported by different authors show some diversity (Hu et al., 2011, 2012; Z. Zhang et al., 2010). Moreover, P-wave tomography shows a seismically fast structure beneath the Sichuan basin up to ~250 km depth (Li et al., 2006), which suggests that the lithosphere beneath the Sichuan basin is probably cold and mechanically strong compared to surrounding regions (Burchfiel et al., 2008). Above ~250 km depth, the eastern Tibetan plateau region is seismically slow, probably indicating lower mechanical strength and elevated temperatures in the lithosphere (Li et al., 2006). The distribution of heat flow in the continental China also demonstrates that the heat flow in eastern Tibet is remarkably higher than that in the Sichuan basin (Hu et al., 2000; Tao and Shen, 2008). Such significant lateral variations in seismic and thermal structures can place important constraints on the rheological properties of the lithosphere and thus may provide insight into the formation mechanism of the eastern Tibetan margin.

3. Data set

Our study mainly involves three types of data: (1) surface heat flow, (2) crustal P-wave velocity distribution from wide-angle seismic profiling, and (3) seismicity data recorded during 1970 to 2012.

The distribution of the available heat flow data is quite uneven in the continental China with a dense coverage in eastern China and poor coverage in western China (Hu et al., 2000). In the eastern Tibetan Plateau, the heat flow data are especially sparse. In order to make our geothermal study reasonable, we adopt a new heat flow map produced by Tao and Shen (2008), which was developed with an objective and integrated interpolating method, taking account of the uniformity within tectonic units and the coherency of regional heat flow, on the basis of a compilation of 6980 heat flow measurements in the Chinese continent and its adjacent areas. In general, the overall heat flow data exhibits high values in eastern China and the Tibetan Plateau, and low in the central and northwestern China (Fig. 2). In contrast to the hot eastern Tibet, the heat flow in the Sichuan basin ranges from 35.2 to 68.8 mW/m^2 with an average of 53.2 mW/m^2, which is typical of a cratonic basin (Xu et al., 2011b; Yuan et al., 2006). This pattern is further confirmed by a recent new release of heat flow data, which showed the local heat flow in the Songpan–Ganze terrane can be as high as

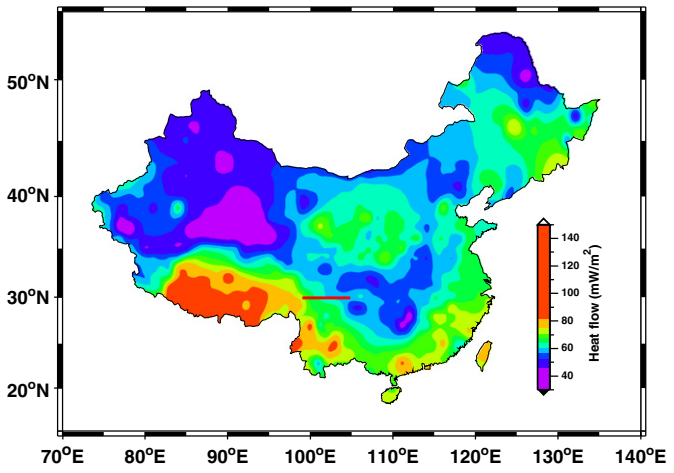

Fig. 2. Heat flow map of continental China. The data are derived from Tao and Shen (2008). The red line indicates the wide-angle seismic profile used in this study.

94.7 mW/m^2, and the heat flow in front of the Longmen Shan is only 63.8 mW/m^2 (Xu et al., 2011a).

The crustal P-wave velocity model used in this study is derived from a wide-angle seismic profile reported by Wang et al. (2007). This profile trends E–W along latitude 30° N and stretches from the Songpan–Ganze terrane in the west to the Sichuan basin in the east (Fig. 1). The seismic velocity model suggests that the eastern Tibet and the Sichuan basin have crustal thicknesses of 62 and 43 km respectively, average crustal P-wave velocities of 6.27 and 6.45 and lower crust (V_p > 6.5 km/s) thicknesses of 27 and 15 km, respectively (Fig. 3b; Wang et al., 2007). Gravity modeling indicates that the eastern Tibet is less dense than the Sichuan basin both in the lower crust and the uppermost mantle (Fig. 3c; Wang et al., 2007; J.S. Zhang et al., 2010). Such lateral variations in crustal structure probably have important effects on its rheological properties. The crustal P-wave velocity model provides important constraints to the compositional, structural and thermal information of the crust, which forms the basis of this study.

The rheological properties of the crust can also be assessed by the seismogenic layer, where earthquakes occur, revealed by seismicity (e.g., Panza and Raykova, 2008; Wu and Zhang, 2012; Zhang et al., 2013). The maximum earthquake depth may be not a direct proxy to the brittle–ductile transition (BDT) depth, but it is expected to be linked to depth-dependent brittle strength (Burov, 2011). For example, Jackson (2002) argued that the depth of seismicity is limited by the

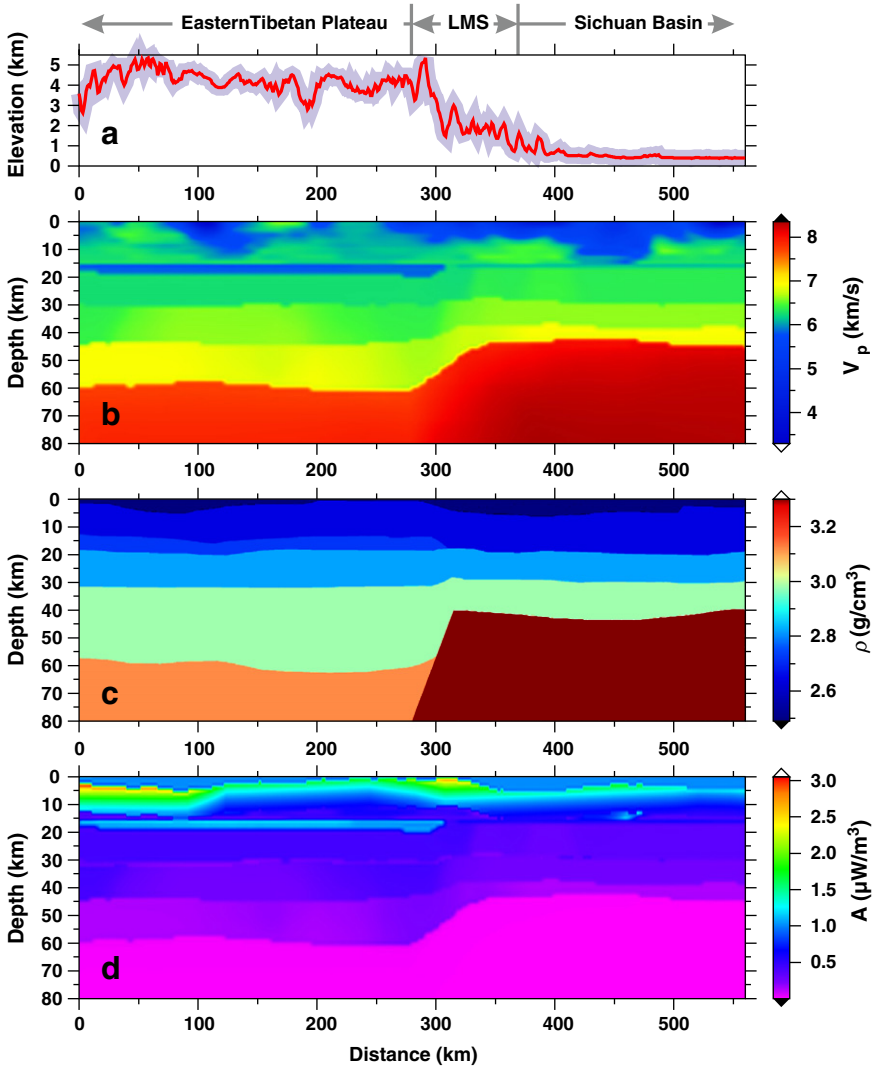

Fig. 3. Geophysical properties of the crust and upper mantle along the profile L1. (a) Topography; (b) crustal P wave velocity model (Wang et al., 2007); (c) crustal density model (Wang et al., 2007); (d) Heat production model converted from the crustal velocity model. The location of the profile is shown in Fig. 1.

BDT depth based on interpretation of yield stress envelopes derived for geological strain rates (~10^{-17} to 10^{-15} s^{-1}). Although a number of studies do not find any obvious relationship between the seismogenic layer and the long-term strength of the lithosphere (Chen et al., 2012; Handy and Brun, 2004; Watts and Burov, 2003), seismicity may reflect the short-term rheology of the lithosphere, which can provide insight into the rheological behavior of the lithosphere at different time scales. For this purpose, we used the seismic events reported by China Earthquake Networks Center (CENC) during the period of 1970 to 2012, and analyzed the depth distribution of earthquakes in terms of 1° by 1° contiguous cells. According to CENC, the accuracy of seismic events is scaled as level A (with an uncertainty of focal depth $\delta d \leq 5$ km), B ($5 \leq \delta d \leq 15$ km), C ($15 \leq \delta d \leq 30$ km) and D ($\delta d \geq 30$ km). In order to make such a study reliable, we only select the events of good quality (level A). The station intervals in this region range from 30 to 60 km. There are a total of 783 events with depth parameter in the study area (99° to 105°E, 29.5° to 29.5°N). It is noteworthy that the location accuracy of seismic events could be influenced by the number of seismic stations, the method of seismic location and the condition of stations at different periods, especially in the early stage. Because we use a large set of data recorded over the past 42 years, the main feature of the focal depth distribution will not be significantly affected.

4. Thermo-rheological modeling

4.1. Governing equations

The bulk strength of the lithosphere is commonly described by the yield strength envelope (YSE, Goetze and Evans, 1979), which predicts the maximum differential stress as a function of depth required to deform the rocks (Ranalli, 1995). YSE allows quantitative assessment of the lithospheric strength based on experimentally determined constitutive equations between brittle and ductile behaviors of rocks (Brace and Kohlstedt, 1980; Burgmann and Dresen, 2008; Kirby, 1983). The YSE concept has been proven to work well as a first-order proxy for evaluating the rheological properties of the lithosphere (Afonso and Ranalli, 2004; Burov, 2011; Handy and Brun, 2004; Jackson, 2002). Thus, YSEs are widely used to validate rock mechanics data and to explain the rheological behavior of the lithosphere in various tectonic environments (Meissner and Mooney, 1998; Muto, 2011; Pauselli et al., 2010; Ranalli and Murphy, 1987; Wang, 2001; Zang et al., 2005; Zhang et al., 2013).

YSEs are constructed by comparing brittle and ductile strengths as a function of depth. At low to moderate temperatures and pressures, rocks are brittle. Because the frictional failure criterion obeys Byerlee's law (Byerlee, 1978), brittle strength is nearly independent of rock type and temperature. In the brittle regime, the frictional shear fracture for most rocks can be adequately described by a linear frictional failure criterion (Sibson, 1974):

$$\sigma_1 - \sigma_3 \equiv \sigma_B = \alpha \rho g z (1-\lambda) \tag{1}$$

where σ_1 and σ_3 are maximum and minimum principal stresses, respectively; σ_B is the critical stress difference in the brittle regime; α is a parameter depending on the type of faulting, with values of 3, 1.2 and 0.75 for thrust, strike–slip and normal faulting, respectively; ρ is the material density; g is the acceleration of gravity; z is depth and λ is the pore fluid factor (ratio of pore fluid pressure to overburden pressure). The most uncertain parameter is the pore fluid pressure. In the absence of information on it, we assume pore fluid pressure is hydrostatic and take a typical value of $\lambda = 0.4$ following as Afonso and Ranalli (2004). Because lithospheric density is heterogeneous, Eq. (1) can be rewritten as

$$\sigma_1 - \sigma_3 \equiv \sigma_B = \alpha g (1-\lambda) \int_0^z \rho(z) dz \tag{2}$$

At greater depths, temperature and strain rate-dependent creep processes start to dominate (Carter and Tsenn, 1987; Kirby and Kronenberg, 1987). In the ductile regime, rocks deform in a manner of power–law dislocation creep (Ranalli, 1995). The experimentally determined flow law for most crustal and upper mantle rocks results in a creep strength given by Kirby (1983):

$$\sigma_1 - \sigma_3 \equiv \sigma_D = \left(\frac{\dot{\varepsilon}}{E}\right)^{1/n} \exp\left(\frac{Q}{nRT}\right) \tag{3}$$

where σ_D is the critical stress difference in the ductile regime; $\dot{\varepsilon}$ is strain rate; E is power–law stress constant; n is power–law exponent; Q is activation energy; R is gas constant and T is absolute temperature. Eq. (3) shows the higher the strain rate is, the larger the differential stress is required. It is noteworthy that low-temperature plasticity (LTP) may become predominant at low temperature and high stress settings (e.g., Mei et al., 2010; Ranalli and Adams, 2013). This flow law, observed in dry olivine (Evans and Goetze, 1979; Mei et al., 2010), is characterized by dislocation glide, and is potentially relevant to the ductile deformation of the lithospheric mantle in the foreland of the LMS. However, an estimate of the role of LTP in wet upper mantle rheology and for other lithospheric compositions is unlikely due to the lack of knowledge of the relevant creep parameters (Ranalli and Adams, 2013).

At any depth, the predominant rheological regime (i.e., YSE) is given by

$$YSE = \min\{\sigma_B, \sigma_D\} \tag{4}$$

The total lithospheric strength (TLS) is given by

$$TLS = \int_0^H YSE dz \tag{5}$$

where H is the thickness of the model. In this paper, H is equal to 80 km.

The construction of the lithospheric strength envelope involves combining compositional and structural information (from geological and geophysical data) with estimated geotherms. Thus, the essential prerequisites for the construction of YSEs are knowledge of the composition and rheology of lithospheric layers, and an estimate of temperature as a function of depth. The former information is mainly extended from laboratory rock deformation experiments. The latter can be calculated with the constraints of surface heat flow, thermal conductivity and distribution of heat production with depth in the study region (see Section 4.2).

The geothermal calculation here involves the contact areas of two distinct tectonic units. Thus, the lateral heat transfer due to the significant lateral variations in thermal conductivity or heat production should be taken into account. For this purpose, the two-dimension heat conduction equation is required. In steady state, the heat conduction in a two-dimension medium is governed by

$$\frac{\partial}{\partial x}\left(k(x,z)\frac{\partial T}{\partial x}\right) + \frac{\partial}{\partial z}\left(k(x,z)\frac{\partial T}{\partial z}\right) + A(x,z) = 0 \tag{6}$$

where T is temperature, $k(x,z)$ is thermal conductivity, $A(x,z)$ is heat production and x, z are horizontal and vertical coordinates, respectively. It is noteworthy that the assumption of thermal steady state is valid only for old lithospheres. The eastern Tibet and Longmen Shan range are regions of tectono-thermal activity that has been rapid on the timescale for thermal equilibration of the lithosphere, and this activity is likely to have produced transient perturbations in the temperature distribution. However, quantifying these temperature variations requires a much better knowledge of the geodynamic evolution of the region. We adopt the steady-state calculations since the tectonic evolution in the eastern Tibetan margin is too uncertain to calculate

non-steady state temperature distributions. Thermal modeling requires the solution of Eq. (6) with the corresponding boundary conditions.

In the calculation, our model is confined to the domain $0 \le z \le D = 80$ km and $0 \le x \le L = 560$ km. The boundary conditions used in our modeling are a constant temperature at the top, a constant heat flow at the bottom and thermal insulating conditions along the sides of the model, i.e.,

$$T(x, z = 0) = T_0 \tag{7}$$

$$\frac{\partial T(x = 0, z)}{\partial x} = \frac{\partial T(x = L, z)}{\partial x} = 0 \tag{8}$$

$$-k(x, z)\frac{\partial T(x, z = D)}{\partial z} = Q_m(x) \tag{9}$$

where T_0 is surface temperature ($T_0 = 10$ °C) and Q_m is the heat flow at the base of the model. The method for solving the above equations is given in the appendix.

4.2. Model parameters

The construction of thermal–rheological models involves a number of parameters, including thermal and creep parameters for lithospheric materials, which need to be constrained with available data for the study region. The power–law creep parameters for selected lithospheric materials are listed in Table 1. Since the composition of the lower portion of the lithosphere is quite varied, we use two different sets of possible rheological parameters for lower crustal and lithospheric mantle rocks: a strong case where the lower crust is mafic granulite and the lithospheric mantle is dry peridotite, and a weak case where the lower crust is felsic granulite and the lithospheric mantle is wet peridotite (see Table 1).

Another important parameter involved in the construction of the lithospheric rheology model is strain rate $\dot{\varepsilon}$. In most cases, the rheological profiles are constructed on the basis of a constant strain rate, e.g., 10^{-15} or 10^{-16} s^{-1} (Burov and Watts, 2006; Ranalli, 2000; Ranalli and Murphy, 1987; Zhang et al., 2013), rather than being based on the observed or inferred strain rate for a given tectonic region. To well account for the lateral variation in tectonic environments (i.e., eastern Tibet, the Longmen Shan range and the Sichuan basin), the strain rate estimated from GPS data (Zhu and Shi, 2011) is used in this study. Following Zhu and Shi (2011), we use a strain rate of 10^{-15} s^{-1} for eastern Tibet, 6×10^{-16} s^{-1} for the Longmen Shan and 10^{-16} s^{-1} for the Sichuan basin.

Solving Eq. (6) requires the knowledge of the thermal conductivity and heat production distribution within the lithosphere. The gross pattern of thermal conductivity in the lithosphere is controlled by composition, temperature and pressure effects (Chapman, 1986). Although the structural and compositional complexity of the crust indicates a concomitant complexity in physical and thermal properties, it is necessary to generalize a structure for the purpose of computing geotherms. Thermal conductivity of most rocks at crustal conditions varies inversely with temperature according to the relation (Cermak and Rybach, 1982; Chapman, 1986):

$$k = \frac{k_0}{1 + cT} \tag{10}$$

where k_0 is the thermal conductivity at surface conditions and c is an experimentally determined constant. At relatively low temperature, thermal conductivity generally decreases with increasing temperature, i.e., $c > 0$, while at 300–500 °C, when the conductivity of basic rocks varies little with temperature, $c = 0$ (Cermak and Rybach, 1982). At temperatures above 500 °C, the conductivity turns to increase with temperature due to the dominant effect of radioactive heat transfer, i.e., $c < 0$ (e.g., Schatz and Simmons, 1972). The thermal conductivities used in our thermal modeling are listed in Table 2.

Another major parameter involved in thermal modeling is heat production. The decay of K, Th and U is supposed to be the main source of heat within the crust. However, reliable estimates of heat production are difficult to obtain at depths greater than a few thousand meters using common geophysical and geochemical exploration methods (Hasterok and Chapman, 2011). On the basis of numerous laboratory measurements, Rybach and Buntebarth (1984) proposed empirical relationships between P-wave seismic velocity (V_p) and heat production (A), which are believed to be valid for a variety of rocks varying from granite to ultrabasites (Cermak and Bodri, 1986). For Phanerozoic rocks, the A–V_p relationship is

$$\ln A = 13.7 - 2.17V_p \tag{11a}$$

and for Precambrian rocks the relationship is

$$\ln A = 12.6 - 2.17V_p \tag{11b}$$

where A is the heat production in $\mu W/m^3$ and V_p is P-wave seismic velocity in km/s.

In this study, Eqs. (11a) and (11b) were used to evaluate the vertical distribution of heat production. Because these two formulae were established from measurements at room temperature (20 °C) and at a pressure of 100 MPa, thus it is necessary to correct seismic velocities determined from wide-angle seismic profiling to such a condition before the V_p–A conversion applies. For this purpose, the correction factors on the order of 1% proposed by Rybach and Buntebarth (1984) was applied to the crustal P-wave model. Readers are referred to Rybach and Buntebarth (1984) for a detailed description of the correction factor. The heat production within the low-velocity layers are evaluated directly with V_p–A conversion because the seismic reversal is believed to be caused by felsic composition with low velocity. Given that the Sichuan basin is the western part of the Yangtze craton and the eastern Tibet (i.e., the Songpan–Ganze terrane) is a Meso-Cenozic orogen (Wang and Meng, 2009), Eq. (11a) is applied to the eastern Tibetan crust (west of the LMS), while Eq. (11b) is applied to the Sichuan basin crust. The converted heat production model from the P wave velocities along the profile is shown in Fig. 3d.

It is noteworthy that uncertainties in parameters, such as thermal conductivity, heat production and surface heat flow, will limit the accuracy of temperature estimations for the deeper crust and lithosphere and ultimately influence the construction of the rheological model. Chapman (1986) investigated the sensitivity of calculated temperatures

Table 1
Rheological parameters used in the yield strength envelope calculations (after the compilation by Ranalli (1997) and references therein). "W" and "S" indicate weak and strong rheology, respectively.

	Composition	Pre-exponential stress constant, E (MPa^{-n} s^{-1})	Power law exponent, n	Activation energy, Q (KJ mol^{-1})
Upper crust	Wet quartzite	3.2×10^{-4}	2.3	154
Lower crust	Felsic granulite (W)	8.0×10^{-3}	3.1	243
	Mafic granulite (S)	1.4×10^{4}	4.2	445
Lithosphere mantle	Wet peridotite (W)	2.0×10^{3}	4.0	471
	Dry peridotite (S)	2.5×10^{4}	3.5	532

Table 2
Thermal conductivity parameters used for thermal modeling: $k = k_0 / (1 + cT)$.

Material	k_0	c	Reference
Upper crust	3.0	$1.5 * 10^{-3}$	Chapman (1986); Cermak and Bodri (1986)
Lower crust	2.6	$1.0 * 10^{-4}$	Chapman (1986)
Lithospheric mantle	3.5	$-0.25 * 10^{-3}$	Chapman (1986); Cermak and Bodri (1986)

to assumed values of model parameters. According to his study, the single most important factor governing the computation of subsurface temperatures is surface heat flow. A change of 10% in surface heat flow corresponds to temperature changes of between 10% and 15% at deeper crustal and upper mantle depths (Chapman, 1986). The influence of heat production on computed temperatures is depth-dependent. The uncertainties in upper crustal heat production have much stronger effect on temperature estimations than that in lower crust and lithospheric mantle (Hasterok and Chapman, 2011). Thermal conductivity at all levels in the lithosphere has an important effect on computed temperatures, but the effects are complicated by the temperature dependence of conductivity and the observation that temperature effects are negative for most crustal rocks but positive in the mantle (Chapman, 1986). An underestimation of upper crustal thermal conductivity will result in an overestimation of temperature at the Moho, but this in turn yields an overestimation of mantle conductivity with a compensating lower thermal gradient (Chapman, 1986). In this study, surface heat flow data are derived from observations, thus they are well-constrained. Heat production model is constructed with P-wave seismic velocity model. Thus the uncertainties in heat production depend on the accuracies of the empirical formula Eqs. (11a) and (11b) and crustal P-wave velocity model.

5. Thermo-rheological structure

The estimated present-day temperature structure of the lithosphere along the profile, together with the observed surface heat flow and the predicted surface and basal heat flow, is shown in Fig. 4. As addressed in Appendix A, the solution of temperature field requires an inverse problem to be solved first, i.e., to find the heat flow at the base of the model (Q_m). Theoretically, it is possible to attain a Q_m-distribution corresponding to any surface heat flow pattern for any required accuracy; however, at the expense of unrealistic horizontal heat flow gradients. In this study, we combine variable separation and Tikhonov regularization techniques (see Appendix A for detail) to overcome the non-uniqueness and instability of the solution. The lateral variation of Q_m has been carefully appreciated with respect to the tectonic structure of the eastern Tibetan margin. After a number of trial and error, we obtain an acceptable compromise of Q_m distribution between the fitting accuracy of the surface heat flow (5 mW/m^2) and lateral variation of basal heat flow (see Fig. 4b). A high temperature anomaly occurs at the uppermost mantle beneath eastern Tibet, basically reconciling with the variation of Q_m (Fig. 4c). The Moho temperature along the profile shows a significant lateral change, which varies from over 800 °C beneath eastern Tibet to ~650 °C beneath the Sichuan basin, with a sharp lateral temperature gradient at the LMS (Fig. 4c). It is clear that the crust in eastern Tibet is hotter on the average than that beneath the Sichuan basin. This is consistent with the findings that Alkali-rich magmatic rocks were erupted in eastern Tibet region from early Cenozoic to Pliocene time, indicating anomalously high temperatures at the base of, and probably throughout, the crust of the eastern Tibetan Plateau (Holbig and Grove, 2008).

The constructed rheological structures are shown in Fig. 5 (weak case) and Fig. 6 (strong case). In the weak case (felsic granulite lower crust and wet peridotite uppermost mantle), the eastern Tibet side has two load-bearing layers, one of which is frictional, restricting to the first ~10 km of the upper crust, the other ductile, concerning the topmost a few kilometers of the lower crust (Fig. 5). The lithosphere beneath the Sichuan basin has a similar rheological structure (Fig. 5), but the ductile creep strength at the top of lower crust and lithospheric mantle exhibits relatively higher values (~300 MPa and ~150 MPa, respectively; see Fig. 5d). Although the rheological profiles of both sides belong to "crème brulée" regime, in which the rheological strength of the lithospheric mantle is negligible, there is a clear lateral variation in rheological structure along the profile. The strength of the lower crust and lithospheric mantle enhances going from eastern Tibet to the Sichuan basin (Fig. 5). This variation is explicitly demonstrated in the values of total lithospheric strength under the compression regime, which changes from 3.5 TN m^{-1} at 150 km of the profile (standing for

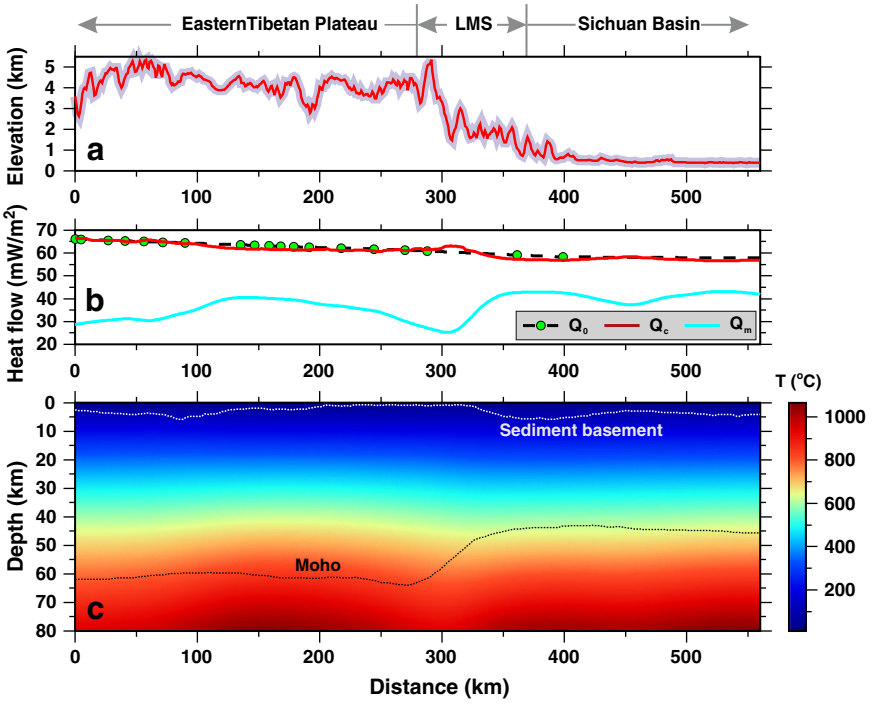

Fig. 4. The estimated crustal thermal structure along the profile L1. (a) Topography; (b) comparison of model-predicted heat flow to the observed ones; (c) modeled crustal temperature structure. Q_0, observed heat flow data; Q_c, model-predicted heat flow; Q_m, resultant model basal heat flow, input from the model bottom. Thermal modeling mainly involves repeatedly adjusting Q_m to make Q_c best fit Q_0.

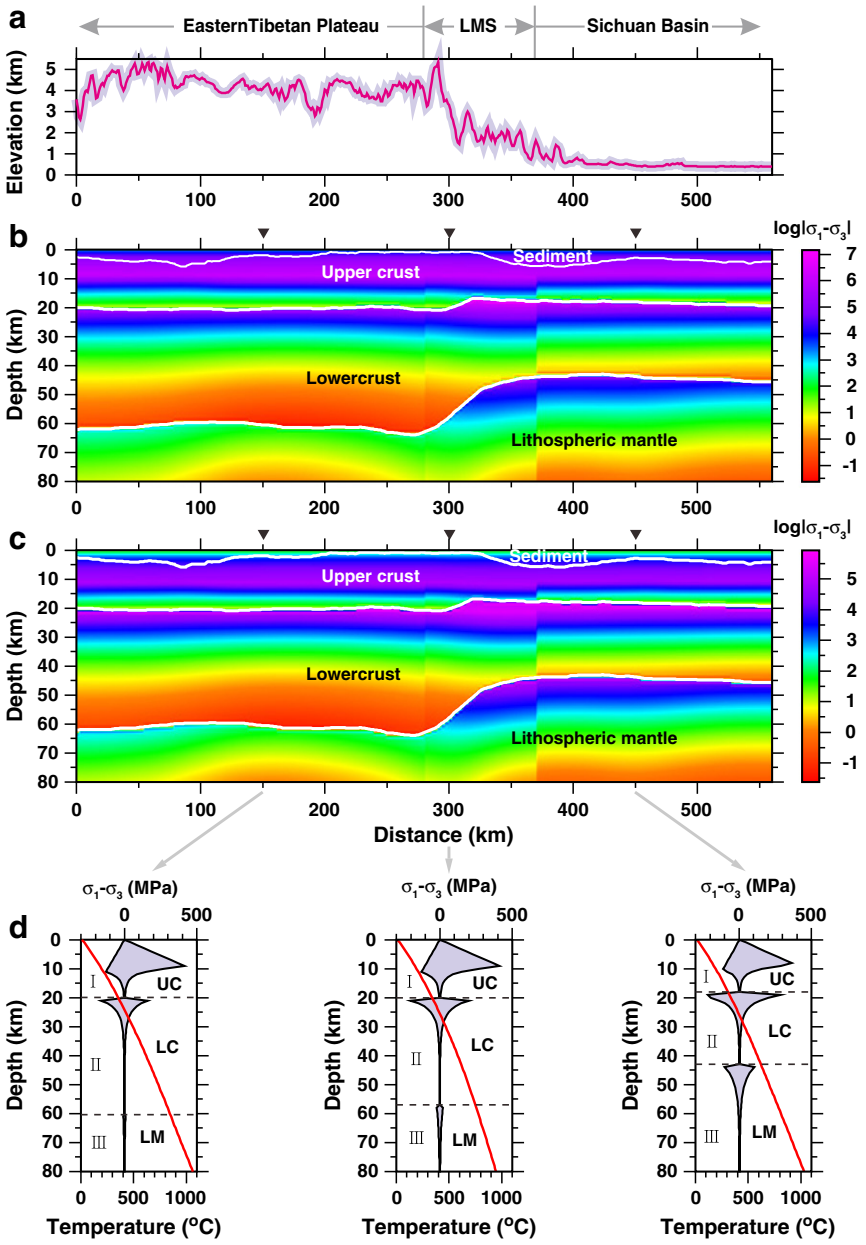

Fig. 5. The constructed 2D rheological strength along the profile (weak case). (a) Topography; (b) 2D lithospheric rheological strength in a compression environment; (c) 2D lithospheric rheological strength in a tension environment; (d) typical rheological profiles at the locations of 150, 300 and 450 km, each of which is accompanied with the corresponding geotherm (red line). The dashed lines indicate the interfaces of upper crust and Moho. UC, upper crust; LC, lower crust; LM, lithospheric mantle. I, II and III denote a composition of wet quartzite, felsic granulite and wet peridotite, respectively.

eastern Tibet) to 4.0 TN m^{-1} at 450 km of the profile (standing for the Sichuan basin).

In the strong case (mafic granulite lower crust and dry peridotite uppermost mantle), the eastern Tibet sector has two frictional load-bearing layers, one of which resides in the topmost ~8 km of the upper crust and the other one occurs at the topmost ~10 km of the lower crust. The Sichuan basin has a similar crustal rheological profile as the eastern Tibet (Fig. 6) except for the topmost few kilometers of the lithospheric mantle, which has significant rheological strength with a peak strength approximately 1000 MPa under the compression stress, even with a few kilometer frictional field in tensional stress (Fig. 6d). In this case, the Moho acts as a major rheological discontinuity beneath the Sichuan basin (Fig. 6d). For the compression regime, TLS varies from 14.4 TN m^{-1} at 150 km of the profile to 20.9 TN m^{-1} at 450 km of the profile. Again, there is an obvious lateral variation in rheological strength along the profile, but this time it changes from a "crème brulée" regime in eastern Tibet to a "jelly sandwich" regime in the Sichuan basin.

In both cases, it is clear that there is a significant lateral variation in the rheological strength of the lithospheric mantle, which changes from a rather weak regime into a fairly strong regime going from eastern Tibet to the Sichuan basin, with an abrupt transition beneath the LMS (see Figs. 5d and 6d). In summary, the lithosphere beneath eastern Tibet is consist of two competent layers, both of which are within the crust, while the lithosphere beneath the Sichuan basin is consist of three competent layers, two of which are in the crust and one is in the topmost lithospheric mantle. Our rheological model clearly shows that the rheological strength of the lithospheric mantle beneath eastern Tibet is weak and negligible, but the lithospheric mantle strength significantly enhances in the Sichuan basin. The result is consistent with the observations that (1) the eastern Tibet region is seismically slow in P-wave velocity and the Sichuan basin is seismically

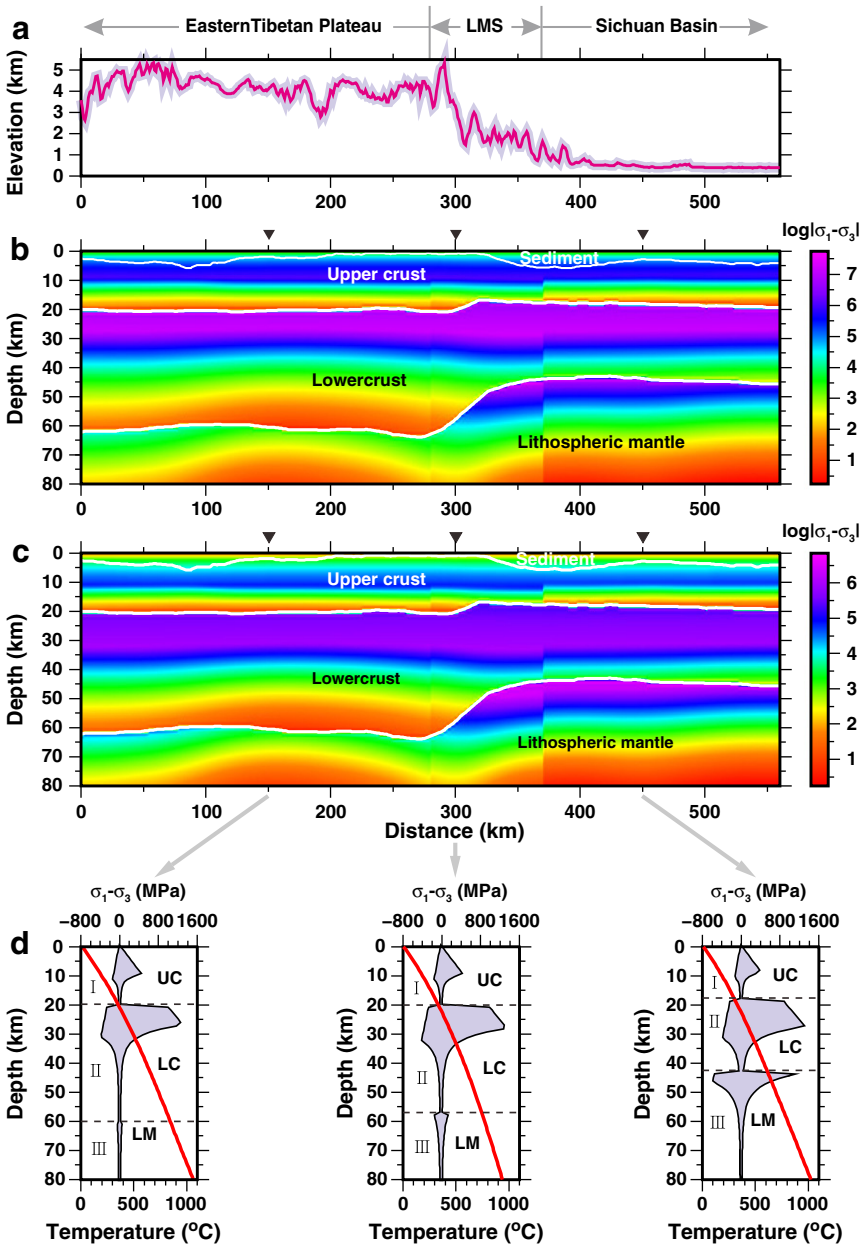

Fig. 6. The constructed 2D rheological strength along the profile (strong case). (a) Topography; (b) 2D lithospheric rheological strength in a compression environment; (c) 2D lithospheric rheological strength in a tension environment; (d) typical rheological profiles at the locations of 150, 300 and 450 km, each of which is accompanied with the corresponding geotherm (red line). The dashed lines indicate the interfaces of upper crust and Moho. UC, upper crust; LC, lower crust; LM, lithospheric mantle. I, II and III denote a composition of wet quartzite, mafic granulite and dry peridotite, respectively.

fast extending to ~250 km depth (Li et al., 2006); and (2) eastern Tibet has low Pn velocities (<7.8 km/s) and the Sichuan basin has high Pn velocities (>8.1 km/s), suggesting a relatively weak uppermost mantle beneath eastern Tibet and a strong uppermost mantle beneath the Sichuan basin (Z. Li et al., 2012).

The lateral differences in rheological structure along the profile are also reflected in the distribution of seismicity occurred in the area from N29.5° to 30.5° along the profile (Fig. 7). The cut-off depth of the seismicity deepens going from eastern Tibet to the Sichuan basin with the deepest earthquakes in front of the LMS range. The seismicity beneath the interiors of eastern Tibet and the Sichuan basin is sparse. Most earthquakes distribute at the conjunct zone between eastern Tibet and the Sichuan basin, where the seismicity is related to major faults (P.Z. Zhang et al., 2010). This could be explained by ductile deformation being predominant beneath eastern Tibet and fault-related brittle deformation being focused in the LMS region because the Tibetan crust is much hotter than that in the LMS and Sichuan basin. For each sub-block, we computed the total energy released by the earthquakes, grouping hypocenters in 4-km intervals. The energy distribution with depth (i.e., log $E - z$) is shown in Fig. 7b. For the purpose of comparison, the logarithm of the energy for the grouped hypocenters is normalized to the maximal value log E_{max} for each sub-block (labeled at the bottom, e.g., Fig. 7b). It is clear that the largest energy release along the profile occurred at the LMS (Fig. 7b). Notably, there are rare earthquakes that occurred at a depth of over 30 km in eastern Tibet. This is in good agreement with the BDT depths of the rheological profile in eastern Tibet (Fig. 6d), and also in accord with the observations that (1) the structure responsible for the 2008 Wenchuan earthquake is a listric reverse fault that tilts ~70° above 15-km depth, then tilts 30° to 40° beneath ~15-km depth, and finally root into the subhorizontal

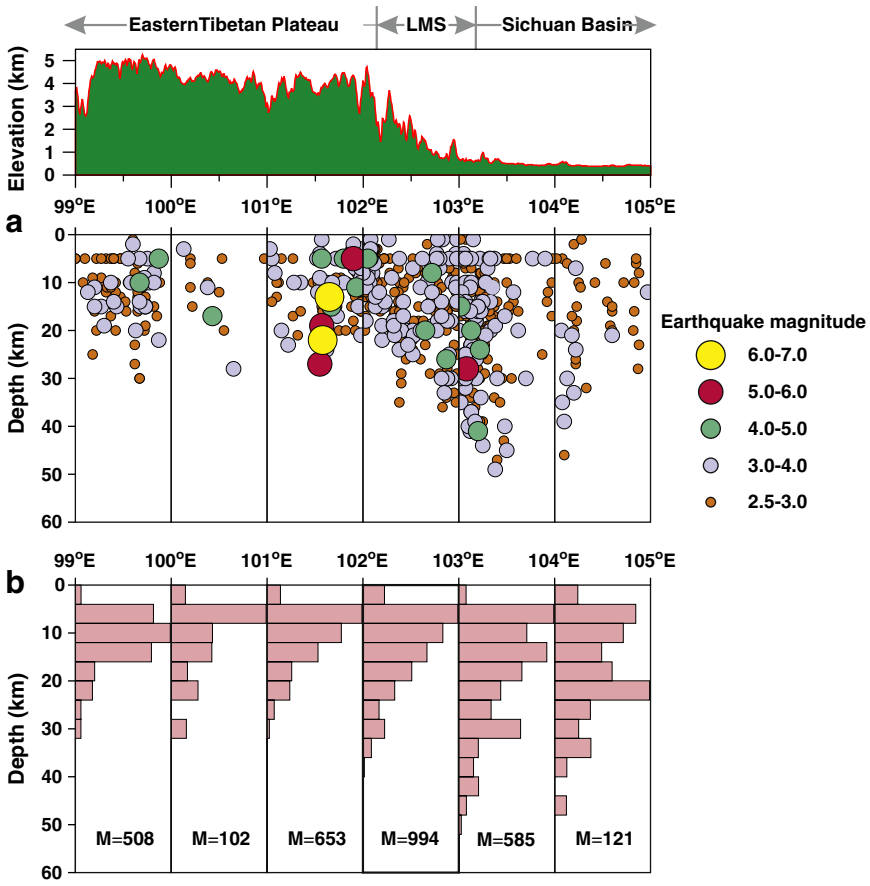

Fig. 7. Seismicity distribution along the profile. (a) the distribution of seismicity from 1970 to 2012 in the area from N29.5° to 30.5° along the profile; (b) seismic energy distribution normalized by $M = \log E_{max}$. The maximum energy release is shown at the bottom of each sub-block.

BDT zone below a depth of 20 to 22 km (P.Z. Zhang et al., 2010); and (2) a high electrical conductivity zone at a depth of 20–40 km only exists on the eastern Tibet side (e.g., profile P3 in Bai et al. (2010)).

Both earthquake distribution and thermo-rheological modeling indicate that the lower crust is weak in eastern Tibet and strong in the Sichuan basin. This is consistent with the general idea of older crust having stronger lower crust.

6. Discussion and conclusions

6.1. Lateral variations in the thermo-rheological structure

Here we use a variety of observations, including the crustal P wave velocity structure, heat flow and seismicity, to construct the thermal/rheological models of the lithosphere along a 30°N wide-angle seismic profile across the eastern Tibetan margin. Two types of lithologic combination are considered: a weak case where the lower crust is felsic granulite and the lithospheric mantle is wet peridotite, and a strong case where the lower crust is mafic granulite and the lithospheric mantle is dry peridotite. In the case of weak rheology, the rheological profile is of the "crème brulée" type (Burov and Watts, 2006), with one frictional load-bearing layer in the top half of the upper crust and one ductile load-bearing layer in the uppermost few kilometers of the lower crust, contributing almost all the lithospheric strength. In the strong case, there are two frictional load-bearing layers in the crust of eastern Tibet, and three load-bearing layers in the Sichuan basin, with two in the crust and one in the uppermost mantle, indicative of "jelly sandwich" type (Burov and Watts, 2006). In this case, the rheological regime changes from the "crème brulée" type in eastern Tibet into marginal "jelly sandwich" type in the Sichuan basin. Both cases show a clear lateral variation in the rheological strength of the lithospheric mantle, which is negligible beneath eastern Tibet but becomes significant strong beneath the Sichuan basin with an abrupt transition underneath the LMS.

The inferred lateral variations in the lithospheric rheological strength along the profile verifies the conclusions by Afonso and Ranalli (2004) that the difference between the "jelly sandwich" and "crème brulée" models is not incompatible, rather "jelly sandwich" and "crème brulée" models are only the end members of a continuous spectrum of possible rheological behaviors, depending on lithospheric temperature, composition and structure.

6.2. Implication for the growth of the eastern Tibetan margin

The eastern Tibetan margin adjacent to the Sichuan basin is characterized by a strikingly steep topography gradient. It was formed in an intra-continental convergence setting, but there is much uncertainty over whether it was formed by upper crustal shortening or lower crustal flow Hubbard and Shaw, 2009; Royden et al., 1997 (Chen et al., 2013a, b;). Z. Zhang et al. (2010) used receiver function to show that the LAB depth decreases from 120 to 150 km beneath the Sichuan basin to 70 to 80 km beneath eastern Tibet and the 410 km discontinuity is depressed below eastern Tibet by ~30 km, suggesting a delamination or removal of the lithosphere root by an eastward asthenospheric escape flow. A more recent S receiver function study conducted in the eastern Tibet region by Hu et al. (2011) also indicated that the LAB depth

beneath eastern Tibet (100 to 120 km) is significantly shallower than that beneath the Sichuan basin (130 to 170 km), although the amount of LAB depth shows some diversity in comparison with the results reported by Z. Zhang et al. (2010).

The inferred thermal/rheological models along the profile demonstrate: (1) one high temperature anomaly exists within the uppermost mantle on eastern Tibet, and the crust in eastern Tibet is remarkably warmer than that in the Sichuan basin; (2) the rheological strength of the lithospheric mantle beneath eastern Tibet is much weaker than that beneath the Sichuan basin. By combining these results with the observations on the crustal/lithospheric architecture in the eastern Tibetan margin (Hu et al., 2011; Robert et al., 2010; Wang et al., 2007; Zhang et al., 2009; Z. Zhang et al., 2010), we construct an integrated lithospheric model as shown in Fig. 8a. The LAB depth is taken from Hu et al. (2011), and the crustal layering is taken from Wang et al. (2007). Two asthenospheric bulges can be observed along the profile: one is underneath eastern Tibet and the other is beneath the LMS (Fig. 8a). This is in good agreement with the observations that two high velocity anomalies exist in the upper mantle beneath eastern Tibet (Bai et al., 2011), indicating possible ongoing lithospheric delamination.

The concept of delamination, defining as detachment of thickened lithospheric mantle from overlying crust during continental collision, was first introduced by Bird (1978, 1979). It has been generalized to include a broad range of processes, including detachment of oceanic slabs (Davies and von Blackenburg, 1995; Sacks and Secor, 1990) and foundering of dense mafic lower crust or upper mantle into less dense asthenosphere driven by phase changes (Kay and Kay, 1993; Meissner and Mooney, 1998). The main consequences of the delamination of thickened lithospheric mantle includes: a regional uplift owing to excess pressure brought by newly risen asthenosphere, increased heat flow, reduced seismic velocities and mafic magmatism (Bird, 1979). Comparing with the Sichuan basin, eastern Tibet manifests high elevation, shallow LAB depth (Hu et al., 2011, 2012; Z. Zhang et al., 2010), low Pn velocity (Z Li et al., 2012), high heat flow (Xu et al., 2011a), active magmatism (Holbig and Grove, 2008) and the weak rheological strength of the lithospheric mantle beneath eastern Tibet, in agreement with the predictions of lithospheric delamination (Bird, 1979). Collectively, we postulate the tectonic process for the growth of the eastern Tibetan margin as follows:

The eastward extrusion of the Tibetan lithosphere was blocked by the rigid Sichuan basin, which leaded to the lithosphere being continuously thickened beneath eastern Tibet. The thickened lithospheric mantle root was delaminated or foundered owing to convective instability or other mechanisms. As a result, the eastern Tibetan margin was regionally uplift relative to the Sichuan basin due to excess pressure brought by newly risen asthenosphere (Fig. 8b, c).

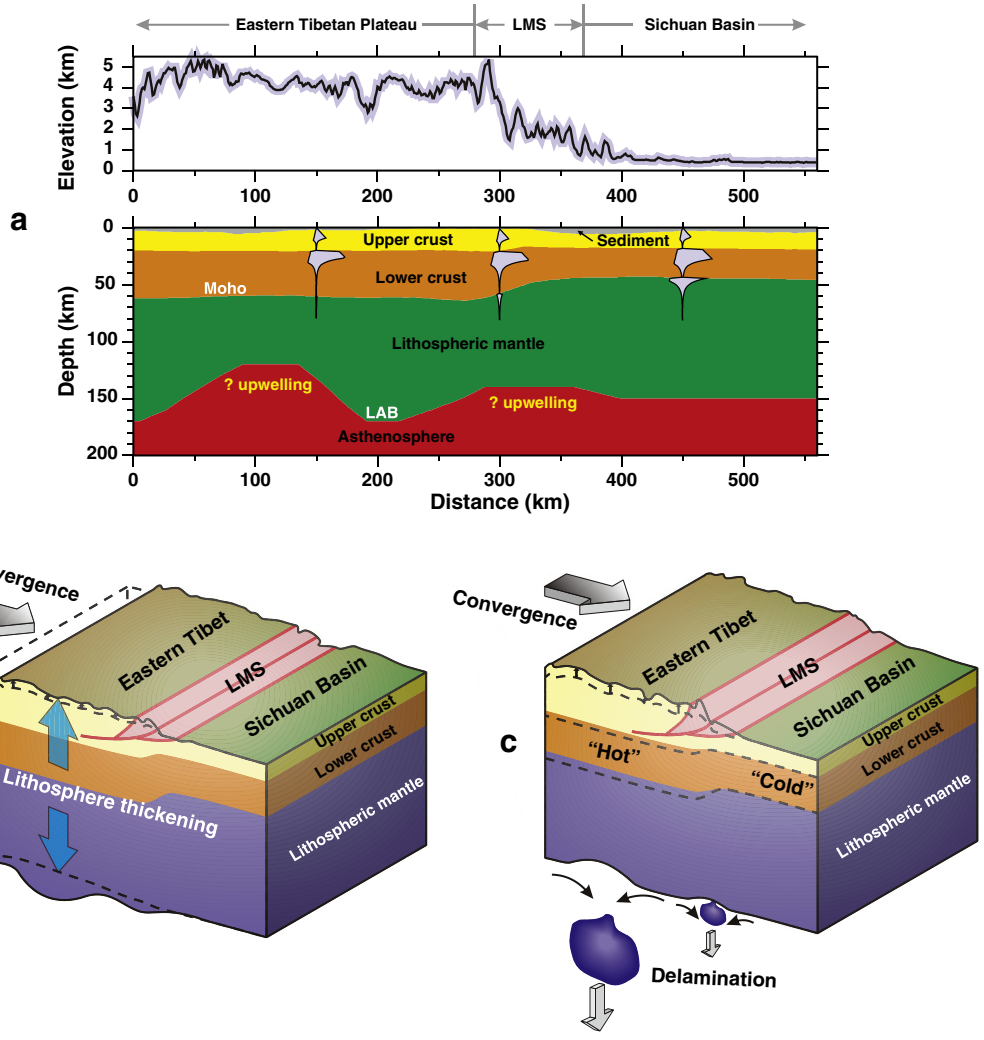

Fig. 8. An alternative tectonic model for the growth of the eastern Tibetan margin. a: the present-day lithosphere architecture beneath the profile L1, showing two bulges on the LAB beneath eastern Tibet (see Fig. 1 for its location). For comparison, the inferred rheological envelopes are integrated into it. The upper crustal, crustal and lithospheric structures are derived from P.Z. Zhang et al. (2010), Wang et al. (2007) and Hu et al. (2011), respectively. b and c: schematic diagram illustrating the growth of the eastern Tibetan margin due to lithospheric mantle delamination. The dashed contour indicates the pre-thickened lithosphere shape.

Acknowledgments

This research was supported by the National Natural Science Foundation of China (Nos. 41004039, 41021063, 41174075, and 41374064), the Ministry of Science and Technology of China (No. 2011CB808904) and the Ministry of Land and Resources of China (SinoProbe-02-02 or 201011041, SinoProbe-03-02 or 201011047). We are grateful to Tao Wei for providing the gridded heat flow data and Zhu Shaobiao for providing the strain rate data. We thank Bai Zhiming and Deng Yangfan for providing the digitized data of the wide-angle seismic profile. Figs. 1–6 were generated with GMT package developed by Paul Wessel and Walter H. F. Smith. We thank an anonymous reviewer, Giorgio Ranalli, and Guest Editor José Badal and M. Santosh for thorough and constructive reviews that greatly improved the manuscript.

Appendix A. Numerical method

The main difficulty in constructing the thermo-rheological model lies in the uncertainty of the heat flow (Q_m) at the base of the model, which serves as the lower boundary condition of the governing equation for the temperature Eq. (5). Therefore, the first goal of our numerical method is to estimate Q_m under the constraints of the given surface temperature (T_0) and heat flow (Q_0).

The solution of Eq. (5) with boundary conditions given in Eqs. (6) to (8) requires the solution of the inverse problem, in which the observed surface heat flow Q_0 can be used to evaluate the heat flow at the base of the model Q_m. This is a Cauchy problem that, as mentioned previously (Engl et al., 1996), is ill-posed in the sense that small measurement errors may be magnified and can completely dominate the solution. By repeated calculation of the surface heat flow corresponding to the model, Q_0', starting with an arbitrary value of Q_m and successively correcting the calculated Q_m by the difference $(Q_0 - Q_0')$, it is possible to evaluate the lower boundary condition of the model within a certain limit of accuracy. Several slightly different approaches to this problem have been discussed by various authors and tested in different tectonic environments (Cermak and Bodri, 1986; Safanda, 1985; Stromeyer, 1984). Alternatively, here we solve the ill-posed problem by decomposing it into several well-posed problems. We assume that the result of the modeling work is a functional relation of the following form:

$$[T(x,z), Q_0] = FDMSolv(T_0, Q_m, k, A). \tag{a1}$$

The above function is implemented by solving the governing Eq. (5) using the finite difference method. The output is the resultant temperature field $T(x,z)$ and surface heat flow Q_0. Our solution method for the inverse problem is based on reusing the above function.

Note that the functions and are function (a1) is not linear because of the source term $A(x,z)$. Thus we first split the solution into two components,

$$T(x,z) = T_1(x,z) + T_2(x,z), Q_0 = Q_{1,0} + Q_{2,0} \tag{a2}$$

where $T_1(x,z)$ satisfies the governing equation with the correct surface temperature T_0 and a zero basal heat flow, i.e., $Q_{1,m} = 0$. The second part $T_2(x,z)$ is obtained by setting $A(x,z) = 0$ in the governing equation and using a zero surface temperature, i.e., $T_{2,0} = 0$, and the correct basal heat flow $Q_{2,m} = Q_m$. The $Q_{1,0}$ and $Q_{2,0}$ correspond to the resultant surface heat flow of the two temperature components (i.e., $T_1(x,z)$ and $T_1(x,z)$). Hence

$$\left[T_2(x,z), Q_{2,0}\right] = FDMSolv(0, Q_m, k, 0). \tag{a3}$$

This defines a linear mapping $Q_{2,0} = K \cdot Q_m$. Using the finite difference method both vectors $Q_{2,0}$ and Q_m and the matrix K can be computed by solving well-posed boundary value problems, i.e.

$$[T_2(x,z), K(:,i)] = FDMSolv(0, e_i, k, 0) \tag{a4}$$

where e_i is the ith standard basis vector, and $K(:,i)$ is the i th column of the matrix K. The linear system of equations $KQ_m = Q_{2,0}$ is ill-conditioned and regularization is needed. Using Tikhonov regularization (Engl et al., 1996) we minimize

$$\left\|KQ_m^{\lambda} - Q_{0,2}\right\|_2^2 + \lambda^2 \left\|Q_m^{\lambda}\right\|_2^2 \tag{a5}$$

where the regularization parameter λ controls the trade-off between accuracy, i.e. keeping the residual small, and stability, i.e. reducing the influence of random errors in the data small. The appropriate value for the parameter λ is selected using the L-curve criterion (Hansen and O'Leary, 1993; Lawson and Hanson, 1974), where both $\|Q_m^{\lambda}\|_2$ and $\|KQ_m^{\lambda} - Q_{0,2}\|_2$ are computed for a wide range of values λ and plotted in a loglog-scale. The resulting graph typically resembles an L and the corner often gives good regularization parameters (Hansen, 1997).

References

Afonso, J.C., Ranalli, G., 2004. Crustal and mantle strengths in continental lithosphere: is the jelly sandwich model obsolete? Tectonophysics 394, 221–232.
Aitchison, J.C., Ali, J.R., Davis, A., 2007. When and where did India and Asia collide? J. Geophys. Res. 112, B05423. http://dx.doi.org/10.1029/2006JB004706.
Arne, D., Worley, B., Wilson, C., Chen, S.F., Foster, D., Luo, Z.L., Liu, S.G., Dirks, P., 1997. Differential exhumation in response to episodic thrusting along the eastern margin of the Tibetan Plateau. Tectonophysics 280 (3–4), 239–256.
Bai, D., Unsworth, M.J., Meju, M.A., Ma, X., Teng, J., Kong, X., Sun, Y., Sun, J., Wang, L., Jiang, C., Zhao, C., Xiao, P., Liu, M., 2010. Crustal deformation of the eastern Tibetan plateau revealed by magnetotelluric imaging. Nat. Geosci. 3, 358–362.
Bai, Z., Tian, X., Tian, Y., 2011. Upper mantle P-wave tomography across the Longmenshan fault belt from passive-source seismic observations along Aba–Longquanshan profile. J. Asian Earth Sci. 40, 873–882.
Bird, P., 1978. Initiation of intracontinental subduction in the Himalaya. J. Geophys. Res. 83, 4975–4987.
Bird, P., 1979. Continental delamination and the Colorado Plateau. J. Geophys. Res. 84, 7561–7571.
Brace, W.F., Kohlstedt, D.L., 1980. Limits on lithospheric stress imposed by laboratory experiments. J. Geophys. Res. 85, 6248–6252.
Burchfiel, B.C., Chen, Z., Liu, Y., Royden, L., 1995. Tectonics of the Longmen Shan and adjacent regions, Central China. Int. Geol. Rev. 37, 661–735.
Burchfiel, B.C., Royden, L.H., van der Hilst, R.D., Hager, B.H., Chen, Z., King, R.W., Li, C., Lu, J., Yao, H., Kirby, E., 2008. A geological and geophysical context for the Wenchuan earthquake of 12 May 2008, Sichuan, People's Republic of China. GSA Today 18. http://dx.doi.org/10.1130/GSATG18A.1.
Burgmann, R., Dresen, G., 2008. Rheology of the lower crust and upper mantle: evidence from rock mechanics, geodesy, and field observations. Annu. Rev. Earth Planet. Sci. 36, 531–567. http://dx.doi.org/10.1146/annurev.earth.36.031207.123326.
Burov, E., Watts, A.B., 2006. The long-term strength of continental lithosphere: jelly-sandwich or crème-brulee? GSA Today 16, 4–10.
Burov, E., 2010. The equivalent elastic thickness (Te), seismicity and the long-term rheology of continental lithosphere: time to burn-out "crème brulee"? Insights from large-scale geodynamic modeling. Tectonophysics 484, 4–26.
Burov, E.B., 2011. Rheology and strength of the lithosphere. Mar. Pet. Geol. 28, 1402–1443.
Byerlee, J.D., 1978. Friction of rocks. Pure Appl. Geophys. 116 (4–5), 615–626.
Carter, N.L., Tsenn, M.C., 1987. Flow properties of continental lithosphere. Tectonophysics 136, 27–63.
Cermak, V., Rybach, L., 1982. Thermal conductivity and specific heat of minerals and rocks. In: Angenheister, G. (Ed.), Landolt–Bornstein New Series. Physical Properties of Rocks, V1a. Springer Verlag, Berlin, pp. 305–343.
Cermak, V., Bodri, L., 1986. Two-dimensional temperature modeling along five East-European geotraverses. J. Geodyn. 5, 133–163.
Chapman, Y., 1986. Thermal gradient in the continental crust. In: Dawson, J.B., Hall, J., Wedepohl, K.H. (Eds.), The Nature of the Lower Continental Crust, vol. 24. Geological Society Special Publication, pp. 63–70.
Chen, L., Gerya, T., Zhang, Z., Zhu, G., Duretz, T., Jacoby, W.R., 2013a. Numerical modeling of eastern Tibetan-type margin: influences of surface processes, lithospheric structure and crustal rheology. Gondwana Res. 24, 1091–1107.
Chen, L., Gerya, T.V., Zhang, Z.J., Aitken, A., Li, Z.H., Liang, X.F., 2013b. Formation mechanism of steep convergent intracontinental margins: insights from numerical modeling. Geophys. Res. Lett. 40, 2000–2005. http://dx.doi.org/10.1002/grl.50446.
Chen, Y., Zhang, Z., Sun, C., Badal, J., 2013. Crustal anisotropy from Moho converted Ps wave splitting analysis and geodynamic implications beneath the eastern margin of Tibet and surrounding regions. Gondwana Res. 24, 946–957.
Chen, W.-P., Molnar, P., 1983. Focal depths of intra-continental and intraplate earthquakes and their implications for the thermal and mechanical properties of the lithosphere. J. Geophys. Res. 88, 4183–4214.

Chen, W.-P., Hung, S.-H., Tseng, T.-L., Brudzinski, M., Yang, Z., Nowack, R.L., 2012. Rheology of the continental lithosphere: progress and new perspectives. Gondwana Res. 21, 4–18.
Chen, S.F., Wilson, C.J.L., Worley, B.A., 1995. Tectonic transition from the Songpan–Garze fold belt to the Sichuan Basin, south-western China. Basin Res. 7 (3), 235–253.
Chen, S.F., Wilson, C.J.L., 1996. Emplacement of the Longmen Shan thrust–nappe belt along the eastern margin of the Tibetan Plateau. J. Struct. Geol. 18, 413–430.
Clark, M.K., Royden, L.H., 2000. Topographic ooze: building the eastern margin of Tibet by lower crustal flow. Geology 28, 703–706.
Cloetingh, S., Burov, B.E., 1996. Thermomechanical structure of European continental lithosphere: constraints from rheological profiles and EET estimates. Geophys. J. Int. 124, 695–723.
Davies, J.H., von Blackenburg, F., 1995. Slab breakoff: a model of lithosphere detachment and its test in the magmatism and deformation of collisional orogens. Earth Planet. Sci. Lett. 129, 85–102.
Densmore, A.L., Ellis, M.A., Li, Y., Zhou, R.J., Hancock, G.S., Richardson, N., 2007. Active tectonics of the Beichuan and Pengguan faults at the eastern margin of the Tibetan Plateau. Tectonics 26, TC4005. http://dx.doi.org/10.1029/2006TC001987.
Engl, H., Hanke, M., Neubauer, A., 1996. Regularization of Inverse Problems. Kluwer Academic Publishers, Dordrecht, the Netherlands.
Evans, B., Goetze, C., 1979. Temperature variation of hardness of olivine and its implication for poly crystalline yield stress. J. Geophys. Res. 84, 5505–5524.
Gan, W., Zhang, P., Shen, Z., Niu, Z., Wang, M., Wan, Y., Zhou, D., Cheng, J., 2007. Present-day crustal motion within the Tibetan Plateau inferred from GPS measurements. J. Geophys. Res. 112, B08416. http://dx.doi.org/10.1029/2005JB004120.
Godard, V., Pik, R., Lavé, J., Cattin, R., Tibari, B., de Sigoyer, J., Pubellier, M., Zhu, J., 2009. Late Cenozoic evolution of the central Longmen Shan, eastern Tibet: insight from (U–Th)/He thermochronometry. Tectonics 28, TC5009. http://dx.doi.org/10.1029/2008TC002407.
Goetze, C., Evans, B., 1979. Stress and temperature in bending lithosphere as constrained by experimental rock mechanics. Geophys. J. R. Astron. Soc. 59, 463–478.
Handy, M.R., Brun, J.P., 2004. Seismicity structure and strength of the continental lithosphere. Earth Planet. Sci. Lett. 223, 427–441.
Hansen, P.C., O'Leary, D.P., 1993. The use of the L-curve in the regularization of ill-posed problems. SIAM J. Sci. Comput. 14, 1487–1503.
Hansen, P.C., 1997. Rank-deficient and discrete ill-posed problems: numerical aspects of linear inversion. SIAM Monographs on Mathematical Modeling and Computation.
Harrison, T.M., Copeland, P., Kidd, W.S.F., Yin, A., 1992. Raising Tibet. Science 255, 1663–1670.
Hasterok, D., Chapman, D.S., 2011. Heat production and geotherms for the continental lithosphere. Earth Planet. Sci. Lett. 307, 59–70.
Holbig, E.S., Grove, T.L., 2008. Mantle melting beneath the Tibetan Plateau: experimental constraints on ultrapotassic magmatism. J. Geophys. Res. 113, B04210. http://dx.doi.org/10.1029/2007JB005149.
Hu, S., He, L., Wang, J., 2000. Heat flow in the continental area of China: a new data set. Earth Planet. Sci. Lett. 179, 407–419.
Hu, J., Xu, X., Yang, H., Wen, L., Li, G., 2011. S receiver function analysis of the crustal and lithospheric structures beneath eastern Tibet. Earth Planet. Sci. Lett. 306, 77–85.
Hu, J., Yang, H., Xu, X., Wen, L., Li, G., 2012. Lithospheric structure and crust–mantle decoupling in the southeast edge of the Tibetan Plateau. Gondwana Res. 22, 1060–1067.
Hubbard, J., Shaw, J.H., 2009. Uplift of the Longmen Shan and Tibetan plateau, and the 2008 Wenchuan (M = 7.9) earthquake. Nature 458, 194–197.
Jackson, J., 2002. Strength of the continental lithosphere: time to abandon the jelly sandwich? GSA Today 12, 4–10.
Jackson, J., Mckenzie, D., Priestley, K., Emmerson, B., 2008. New views on the structure and rheology of the lithosphere. J. Geol. Soc. Lond. 165, 453–465.
Jiang, X., Jin, Y., 2005. Mapping the deep lithospheric structure beneath the eastern margin of the Tibetan Plateau from gravity anomalies. J. Geophys. Res. 110, B07407. http://dx.doi.org/10.1029/2004JB003394.
Kay, R.W., Kay, S.M., 1993. Delamination and delamination magmatism. Tectonophysics 219, 177–189.
Kirby, S.H., 1983. Rheology of the lithosphere. Rev. Geophys. Space Phys. 21, 1458–1487.
Kirby, S.H., Kronenberg, A.K., 1987. Rheology of the lithosphere: selected topics. Rev. Geophys. 25, 1219–1244 (and correction 1680–1681).
Kirby, E., Reiners, P.W., Krol, M.A., Whipple, K.X., Hodges, K.V., Farley, K.A., Tang, W., Chen, Z.L., 2002. Late Cenozoic evolution of the eastern margin of the Tibetan Plateau: inferences from $^{40}Ar/^{39}Ar$ and (U–Th)/He thermochronology. Tectonics 21 (1), 1001. http://dx.doi.org/10.1029/2000TC001246.
Lawson, C.L., Hanson, R.J., 1974. Solving Least Squares Problems. Prentice-Hall, Englewood Cliffs, NJ.
Li, Y., Allen, P.A., Densmore, A.L., Qiang, X., 2003. Evolution of the Longmen Shan foreland basin (western Sichuan, China) during the Late Triassic Indosinian orogeny. Basin Res. 15, 117–138.
Li, C., van der Hilst, R.D., Toksoz, M.N., 2006. Constraining spatial variations in P-wave velocity in the upper mantle beneath SE Asia. Phys. Earth Planet. Inter. 154, 180–195.
Li, Z., Ni, S., Hao, T., Xu, Y., Roecker, S., 2012a. Uppermost mantle structure of the eastern margin of the Tibetan Plateau from interstation Pn traveltime difference tomography. Earth Planet. Sci. Lett. 335–336, 195–205.
Li, Z.-W., Liu, S., Chen, H., Deng, B., Hou, M., Wu, W., Gao, J., 2012b. Spatial variation in Meso-Cenozoic exhumation history of the Longmen Shan thrust belt (eastern Tibetan Plateau) and the adjacent western Sichuan basin: constraints from fission tract thermochronology. J. Asian Eart Sci. 47, 185–203.
Liu, S.G., Li, Z.W., Cao, J.X., Liu, S., Deng, B., Wang, G.Z., Deng, B., 2009. 4-D textural and structural characteristics of Longmen intracontinental composite orogenic belt, southwest China. Chin. J. Geol. 44 (4), 1151–1179 (in Chinese with English abstract).
Maggi, A., Jackson, J.A., McKenzie, D., Priestley, K., 2000a. Earthquake focal depths, effective elastic thickness, and the strength of the continental lithosphere. Geology 28, 495–498.
Maggi, A., Jackson, J.A., Priestley, K., Baker, C., 2000b. A re-assessment of focal depth distributions in southern Iran, the Tien Shan and northern India: do earthquakes really occur in the continental mantle? Geophys. J. Int. 143, 629–661.
Mei, S., Suzuki, A.M., Kohlstedt, D.L., Dixon, N.A., Durham, W.B., 2010. Experimental constraints on the strength of the lithospheric mantle. J. Geophys. Res. 115, B08204. http://dx.doi.org/10.1029/2009JB006873.
Meissner, R., Mooney, W., 1998. Weakness of the lower continental crust: a condition for delamination, uplift, and escape. Tectonophysics 296, 47–60.
Molnar, P., Stock, J.M., 2009. Slowing of India's convergence with Eurasia since 20 Ma and its implications for Tibetan mantle dynamics. Tectonics 28, TC3001. http://dx.doi.org/10.1029/2008TC002271.
Muto, J., 2011. Rheological structure of northeastern Japan lithosphere based on geophysical observations and rock mechanics. Tectonophysics 503, 201–206. http://dx.doi.org/10.1016/j.tecto.2011.03.002.
Panza, G.F., Raykova, R.B., 2008. Structure and rheology of lithosphere in Italy and surrounding. Terra Nova 20, 194–199. http://dx.doi.org/10.1111/j.1365-3121.2008.00805.x.
Pauselli, C., Ranalli, G., Federico, C., 2010. Rheology of the Northern Apennines: lateral variations of lithospheric strength. Tectonophysics 484, 27–35. http://dx.doi.org/10.1016/j.tecto.2009.08.29.
Ranalli, G., Murphy, D.C., 1987. Rheological stratification of the lithosphere. Tectonophysics 132, 281–295.
Ranalli, G., 1995. Rheology of the Earth, second ed. Chapman and Hall, London 413.
Ranalli, G., 1997. Rheology of the lithosphere in space and time. In: Burg, J.-P., Ford, M. (Eds.), Orogeny through Time: Geological Society of London Special Publication, 121, pp. 19–37.
Ranalli, G., 2000. Rheology of the crust and its role in tectonic reactivation. J. Geodyn. 30, 3–15.
Ranalli, G., Adams, M., 2013. Rheological contrast at the continental Moho: effects of composition, temperature, deformation mechanism, and tectonic regime. Tectonophysics 609, 480–490.
Robert, A., Zhu, J., Vergne, J., Cattin, R., Chan, L.S., Wittlinger, G., Herquel, G., de Sigoyer, J., Pubellier, M., Zhu, L.D., 2010. Crustal structures in the area of the 2008 Sichuan earthquake from seismologic and gravimetric data. Tectonophysics 491, 205–210.
Royden, L.H., Burchfiel, B.C., King, R.W., Wang, E., Chen, Z., Shen, F., Liu, Y., 1997. Surface deformation and lower crustal flow in eastern Tibet. Science 276, 788–790.
Royden, L.H., Burchfiel, B.C., van Hilst, R.D., 2008. The geological evolution of the Tibetan Plateau. Science 321, 1054. http://dx.doi.org/10.1126/science.1155371.
Rybach, L., Buntebarth, G., 1984. The variation of heat generation, density and seismic velocity with rock type in the continental lithosphere. Tectonophysics 103, 335–344.
Sacks, P.E., Secor, D.T., 1990. Delamination in collisional orogens. Geology 18, 999–1002.
Safanda, J., 1985. Calculation of temperature distribution in the two-dimensional geothermal profile. Stud. Geophys. Geod. 29, 191–207.
Schatz, J.F., Simmons, G., 1972. Thermal conductivity of earth materials at high temperatures. J. Geophys. Res. 77, 6966–6983.
Sibson, R.H., 1974. Frictional constraints on thrust, wrench and normal faults. Nature 249, 542–544.
Stromeyer, D., 1984. Downward continuation of heat flow data by means of the least squares method. Tectonophysics 103, 55–66.
Tao, W., Shen, Z., 2008. Heat flow distribution in Chinese continent and its adjacent areas. Prog. Nat. Sci. 18, 843–849.
Tejero, R., Ruiz, J., 2002. Thermal and mechanical structure of the central Iberian Peninsula lithosphere. Tectonophysics 350, 49–62.
Wang, Y., 2001. Heat flow pattern and lateral variations of lithosphere strength in China mainland: constraints on active deformation. Phys. Earth Planet. Inter. 126, 121–146.
Wang, C.Y., Han, W.B., Wu, J.P., Lou, H., Chan, W.W., 2007. Crustal structure beneath the eastern margin of the Tibetan Plateau and its tectonic implications. J. Geophys. Res. 112, B07307. http://dx.doi.org/10.1029/2005JB003873.
Wang, E.C., Meng, Q.R., 2009. Mesozoic and Cenozoic tectonic evolution of the Longmenshan fault belt. Sci. China Ser. D Earth Sci. 52, 579–592.
Wang, E., Kirby, E., Furlong, K.P., van Soest, M., Xu, G., Shi, X., Kamp, P.J.J., Hodges, K.V., 2012. Two-phase growth of high topography in eastern Tibet during the Cenozoic. Nat. Geosci. http://dx.doi.org/10.1038/NGEO1538.
Watts, A.B., Burov, E., 2003. Lithospheric strength and its relationship to the elastic and seismogenic layer thickness. Earth Planet. Sci. Lett. 213, 113–131.
Wu, J., Zhang, Z., 2012. Spatial distribution of seismic layer, crustal thickness, and Vp/Vs ratio in the Permian Emeishan mantle plume region. Gondwana Res. 22, 127–139.
Xia, L., Li, X., Ma, Z., Xu, X., Xia, Z., 2011. Cenozoic volcanism and tectonic evolution of the Tibetan plateau. Gondwana Res. 19, 850–866.
Xu, M., Zhu, C.Q., Rao, S., Hu, S.B., 2011a. Difference of thermal structure between eastern edge of Tibet Plateau and western Sichuan Basin. Chin. J. Geol. 46, 203–212 ([in Chinese with English abstract]).
Xu, M., Zhu, C.Q., Tian, Y.T., Rao, S., Hu, S.B., 2011b. Borehole temperature logging and characteristics of subsurface temperature in the Sichuan Basin. Chin. J. Geophys. 54, 1052–1060 ([in Chinese with English abstract]).
Yuan, Y.S., Ma, Y.S., Hu, S.B., Guo, T.L., Fu, X.Y., 2006. Present-day geothermal characteristics in South China. Chin. J. Geophys. 49, 1118–1126 ([in Chinese with English abstract]).
Zahirovic, S., Muller, R.D., Seton, M., Flament, N., Gurnis, M., Whittaker, J., 2012. Insights on the kinematics of the India–Eurasia collision from global geodynamic models. Geochem. Geophys. Geosyst. 13, Q04W11. http://dx.doi.org/10.1029/2011GC003883.
Zang, S.X., Wei, R.Q., Liu, Y.G., 2005. Three-dimensional rheological structure of the lithosphere in the Ordos block and its adjacent area. Geophys. J. Int. 163, 339–356. http://dx.doi.org/10.1111/j.1365-246X.2005.02745.x.

Zhang, Z., Wang, Y., Chen, Y., Houseman, G.A., Tian, X., Wang, E., Teng, J., 2009. Crustal structure across Longmenshan fault belt from passive source seismic profiling. Geophys. Res. Lett. 36, L17310. http://dx.doi.org/10.1029/2009GL039580.

Zhang, Z., Yuan, X., Chen, Y., Tian, X., Kind, R., Li, X., Teng, J., 2010a. Seismic signature of the collision between the East Tibetan escape flow and the Sichuan basin. Earth Planet. Sci. Lett. 292, 254–264.

Zhang, J.S., Gao, R., Zeng, L.S., Li, Q.S., Guan, Y., He, R.Z., Wang, H.Y., Lu, Z.W., 2010b. Relationship between characteristics of gravity and magnetic anomalies and the earthquakes in the Longmenshan range and adjacent areas. Tectonophysics 491, 218–229.

Zhang, P.Z., Wen, X.Z., Shen, Z.K., Chen, J.H., 2010c. Oblique, high-angle, listric-reverse faulting and associated development of strain: the Wenchuan earthquake of May 12, 2008, Sichuan, China. Annu. Rev. Earth Planet. Sci. 38, 353–382.

Zhang, Z., Deng, Y., Chen, L., Wu, J., Panza, G., 2013. Seismic structure and rheology of the crust under mainland China. Gondwana Res. 23, 1455–1483.

Zhu, D.-C., Zhao, Z.-D., Niu, Y., Dilek, Y., Hou, Z.-Q., Mo, X.-X., 2013. The origin and pre-Cenozoic evolution of the Tibetan Plateau. Gondwana Res. 23, 1429–1454.

Zhu, S., Shi, Y., 2011. Estimation of GPS strain rate and its error analysis in the Chinese continent. J. Asian Earth Sci. 40, 351–362.